Metrol. Meas. Syst., Vol. 27 (2020) No. 1, pp. 103–117
DOI: 10.24425/mms.2020.131715

METROLOGY AND MEASUREMENT SYSTEMS
Index 330930, ISSN 0860-8229
www.metrology.pg.gda.pl

TWO-WAY ANOVA GAGE R&R WORKING EXAMPLE APPLIED TO SPECKLE INTENSITY STATISTICS DUE TO DIFFERENT RANDOM VERTICAL SURFACE ROUGHNESS CHARACTERISTICS USING THE FRESNEL DIFFRACTION INTEGRAL

Moisés Cywiak[1)], David Cywiak[2)], Etna Yáñez[1)]

1) *Centro de investigaciones en Óptica A.C., Loma del Bosque 115, Colonia Lomas del Campestre, León, C.P. 37150, Guanajuato, México* (✉ *moi@cio.mx*, +52 477 441 4200, *etnay@cio.mx*)
2) *Centro Nacional de Metrología, km 4.5 Carretera a Los Cués, Municipio El Marqués, C.P. 76246, Querétaro, México* (*dcywiak@cenam.mx*)

Abstract

We present computer simulations of a two-way ANOVA gage R&R study to determine the effects on the average speckle width of intensity patterns caused by scattered light reflected from random rough surfaces with different statistical characteristics. We illustrate how to obtain reliable computer data that properly simulate experimental measurements by means of the Fresnel diffraction integral, which represents an accurate analytical model for calculating the propagation of spatially-limited coherent beams that have been phase-modulated after being reflected by the vertical profiles of the generated surfaces. For our description we use four differently generated vertical profiles and five different vertical randomly generated roughness values.

Keywords: speckle pattern, ANOVA and gage R&R, autocorrelation, Fresnel diffraction integral.

1. Introduction

As indicated in the international standard ISO 5725-1:1994 [1] concerning measurement methods, the trueness of a measurement is quantified by a statistical term defined as bias which is basically the difference between the expectation of the test results and an accepted reference value. In general, these differences are well represented by two statistical terms known as repeatability and reproducibility. Thus, when a hypothesis has to be tested experimentally, one of the most reliable and robust accepted methods are the analysis of variances (ANOVA) and the gage repeatability and reproducibility (gage R&R). In this report we give an illustrative working example applied to speckle statistics, illustrating how data obtained by computer simulations based on a well-established analytical model can be used in a way equivalent to that of laboratory experimental data, with no loss of reliability to determine the average speckle width for different reflective rough surfaces.

Speckle intensity patterns that result from the reflection of an illuminating coherent source on a rough surface have many applications in different fields, as the measurement of deformation of large objects [2], studies on rough surfaces [3], astronomy [4], biological tissue imaging [5], studies of coagulation processes [6], acoustics [7] *etc.*

As it is not possible to control exhaustively the roughness characteristics of real materials used in speckle experiments, it becomes necessary to perform calculations based on numerical models to validate some particular findings [8]. Most of the simulations on rough surface models are based on vertical height distributions that follow random Gaussian probability density functions [9] and it is difficult to find reports dealing with non-Gaussian density probability functions as for example is included in [10–12].

It is commonly accepted that the average speckle width does not depend on the statistical profile of the reflecting rough surface that causes an intensity speckle pattern. However, it may be more natural to assume that the statistical characteristics of the vertical profiles of the simulated rough surfaces may affect the average lateral speckle width. To provide a robust answer to this question, in this report we present a two-way analysis of variances (ANOVA) and gage repeatability and reproducibility (R&R) studies, using well-known equations for these methods. We present a complete worked example, applied to evaluate the average speckle width due to the reflection of a spatially-limited coherent beam from random-rough-surfaces with different statistical characteristics. We focus on the shape of the histograms and the autocorrelations of the intensity speckle patterns. For our description, a spatially limited illuminating coherent beam, phase-modulated by reflection from a rough surface, is propagated up to an observation plane by means of the Fresnel diffraction integral. The rough surface profiles considered in this report are obtained by an algorithm that has been described in [13, 14]. This algorithm provides ample flexibility to attain different random characteristics of the simulated surfaces by simply changing the analytical expression of a generating function. In the following sections we describe our ANOVA and gage R&R simulations.

2. Analytical description

2.1. Surface simulation

We begin our description by listing the steps required by the algorithm given in [13, 14] to generate different random rough surfaces. As it will be apparent from the results presented in the following sections, a one-dimensional model will be appropriate for the ANOVA and R&R studies described in this report.

The first step consists in providing an analytical expression of a function $f(x)$ that will generate a surface with a random vertical height distribution. The vertical profile of the surface generated, in turn, will have a corresponding autocorrelation function whose plot will exhibit a central sharp peak. The width of this peak can be approximately set by some parameters defined in the generating function. The only limitation imposed on $f(x)$ is that it has to be a symmetric decaying function [13, 14].

The next step consists in calculating the Fourier transform $F(u)$ of $f(x)$, u being the frequency coordinate that corresponds to the spatial-coordinate x. Then, a so called pupil function is calculated as $P(u) = \sqrt{F(u)}$. Next, a random function $\eta(u)$ with zero mean and uniform distribution is generated and multiplied by the pupil function as $P(u)\,\eta(u)$. The vertical distribution $h(x)$ of the simulated surface is obtained by calculating the inverse Fourier transform of the product $P(u)\,\eta(u)$. At this point it will be noticed that $h(x)$ will be symmetric around the origin; this is not a limitation of the algorithm as it is only necessary to obtain a shifted version of this function by

www.czasopisma.pan.pl PAN POLSKA AKADEMIA NAUK www.journals.pan.pl
Metrol. Meas. Syst., Vol. 27 (2020), No. 1, pp. 103–117
DOI: 10.24425/mms.2020.131715

introducing an appropriate phase term in the Fourier process. Finally the vertical height of $h(x)$ is properly scaled to attain a desired RMS value of the vertical height distribution.

It is important to mention that once a rough surface represented by $h(x)$ is numerically obtained as described above, it has to be plotted for evaluation. If the plot of $h(x)$ exhibits isolated sharp peaks, then this particular function must be discarded as this type of peaks represent flaws or scratches on the corresponding surface altering the diffraction patterns with undesired ripples. Thus, we implemented a numerical routine to discard non-desired surfaces. This routine consists in calculating the magnitude of the maximum and minimum of their corresponding height distributions symmetrically positioned around the horizontal axis. If any of these two amplitudes is greater than three times the RMS value, this surface is discarded. By using this criterion, we found that surfaces exhibiting isolated sharp peaks were efficiently discarded.

Figure 1 depicts a plot of a simulated rough surface free of defects. The vertical profile was properly scaled to attain an RMS value of 0.1 μm.

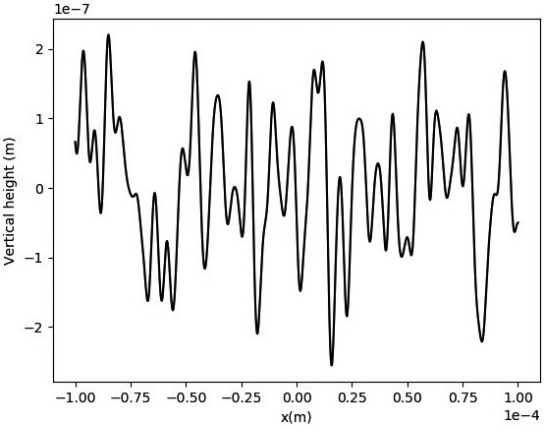

Fig. 1. One of the simulated one-dimensional surfaces with RMS value of 0.1 μm.

The normalized autocorrelation plot that corresponds to the surface of Fig. 1 is plotted in Fig. 2.

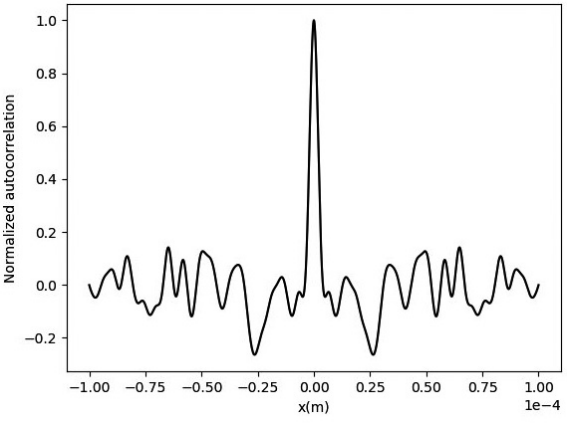

Fig. 2. The normalized autocorrelation corresponding to the surface plotted in Fig. 1. In the following section we describe the optical process and the automated method used to measure the width of the central peak.

2.2. Optical process

Once a set of valid surfaces is properly generated as described above, each surface is placed on an object plane of an optical setup similar to the one depicted in Fig. 3 to illuminate normally a region of the surface by a spatially-limited coherent source.

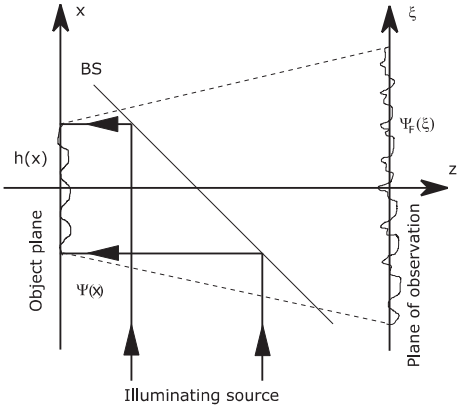

Fig. 3. An optical setup for illuminating and propagating the beam reflected from a numerically generated rough surface (BS is a beam splitter).

On the object plane, the amplitude distribution $\Psi(x)$ of the reflected beam is calculated as:

$$\Psi(x) = \text{rect}\,(x, A)\exp\left[i4\pi h(x)/\lambda\right]. \tag{1}$$

In (1) a rectangle function, rect (x, A) is introduced to spatially limit the extent of the illuminating source on the object plane. The rectangle function is equal to one if $|x| \leq A/2$, and to zero otherwise. The parameter λ is the wavelength of the illuminating source. The plane of observation is placed at a distance z from the object plane. Both planes are parallel to each other. The amplitude of the propagated beam, $\Psi_F(\xi)$, on the plane of observation with the spatial coordinate ξ (Fig. 3) is calculated by means of the one-dimensional Fresnel diffraction integral [15] given as:

$$\Psi_F(\xi) = \frac{1}{\sqrt{i\lambda z}}\exp\left(\frac{i2\pi z}{\lambda}\right)\int_{-\infty}^{\infty}\Psi(x)\exp\left[\frac{i\pi}{\lambda z}(x-\xi)^2\right]\mathrm{d}x. \tag{2}$$

For our simulations we used $A = 200$ μm, $\lambda = 0.6328$ μm and $z = 1$ m.

The intensity distribution, $I(\xi)$, on the plane of observation is calculated by using the amplitude distribution given by (2) as:

$$I(\xi) = \Psi_F(\xi)\Psi_F(\xi)^*. \tag{3}$$

In (3) the symbol $*$ represents conjugation.

Figure 4 depicts one of the normalized intensity distributions of a speckle pattern obtained on the plane of observation.

It should be noticed that in Fig. 4 the observation window has been shifted to one side of the origin. This shifting is introduced intentionally to avoid the contribution of ballistic photons that could alter the statistics of the speckle patterns under study.

Metrol. Meas. Syst., Vol. 27 (2020), No. 1, pp. 103–117
DOI: 10.24425/mms.2020.131715

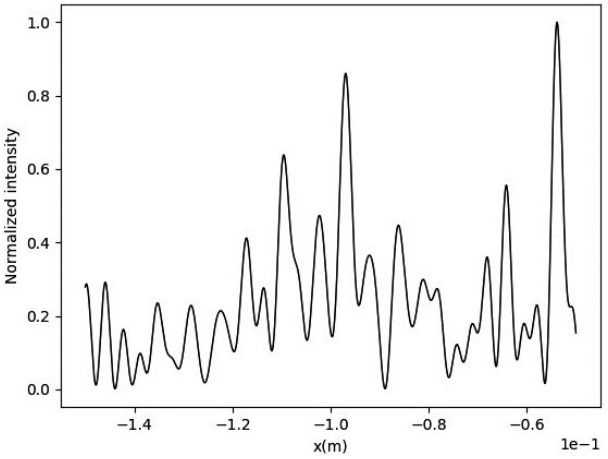

Fig. 4. One of the normalized intensity distributions calculated on the plane of observation by using the one-dimensional Fresnel diffraction integral, for the surface depicted in Fig. 1.

It is worth mentioning that for each intensity distribution obtained on the plane of observation we verified that the intensity histograms follow a decreasing exponential behavior in accordance with well-known analytical equations [16].

Figure 5 depicts a plot of the autocorrelation that corresponds to the intensity distribution on the plane of observation plotted in Fig. 4.

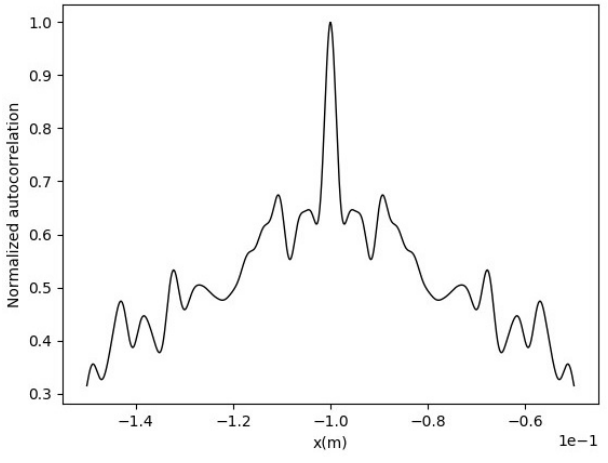

Fig. 5. The normalized autocorrelation for the speckle pattern plotted in Fig. 4.

To calculate a representative value of the width of the central peak of the autocorrelations obtained avoiding possible errors of appreciation of an operator and also to automate the calculations, we implemented a simple numerical method. First, the position of the central peak maximum and the position of the first two minima at both sides of this peak are calculated.

Then, following [16, 17] the horizontal distance between the referred two minima is taken as the autocorrelation width.

The following four different generating functions $f(x)$ were considered:

$$\text{Generator I}: \quad f(x) = \exp\left[-\left(\frac{\sqrt{x^2}}{L}\right)^{2\alpha}\right]; \qquad \alpha = 1.2. \tag{4}$$

$$\text{Generator II}: \quad f(x) = \exp\left[-\left(\frac{\sqrt{x^2}}{L}\right)^{2\alpha}\right]; \qquad \alpha = 0.8. \tag{5}$$

$$\text{Generator III}: \quad f(x) = \left[1 + \frac{1}{N}\left(\frac{x}{L}\right)^2\right]^{-N}; \qquad N = 6000. \tag{6}$$

$$\text{Generator IV}: \quad f(x) = J_0\left(\frac{x}{L}\right). \tag{7}$$

In (7) J_0 is the Bessel function of order zero of the first kind.

The functions given by (4)–(7) were selected to achieve surfaces with the most dissimilar statistical characteristics between them. Although it may seem unusual, a Bessel generating function was included to magnify differences between the random surfaces.

It is important to remark that the value of a typical average speckle width anticipated as $2\lambda z/A = 6.328 \times 10^{-3}$ m [16], does not necessarily have to coincide exactly with the width of the autocorrelation obtained as described above, 5.7×10^{-3} m in the example. The discrepancy obviously obeys statistical reasons and is irrelevant for the statistical purposes presented here. The fundamental factor in our study resides in performing measurements always in strictly the same conditions. Under this assumption, the statistical parameters being measured, such as repeatability and reproducibility, will be demonstrated as highly reliable, as confirmed by the results given in the following sections.

3. ANOVA and gage R&R calculations

To compare the effect that results from using different generating functions $f(x)$ along with different correlations and different RMS roughness values, we used the four different generating functions described in the former section, (4)–(7). For each of the generating functions we assigned five different L values, equally spaced, ranging from 3.0×10^{-6} to 3.8×10^{-6} m. Additionally, there are five different equally spaced RMS values ranging from 1×10^{-7} to 1.8×10^{-7} m as indicated in Tables 1–4.

It is worth mentioning that it would be desirable to present the data arranged in a single table. However, due to the limitation of space, the data are presented in four tables instead of only one. Each entry in the tables represents the average autocorrelation width of 20 processes. Each process comprises: generation of a random surface profile, reflection of the illuminating beam from the generated surface, propagation of the reflected beam up to the plane of observation by means of the discrete Fresnel diffraction integral, calculation of the intensity distribution on the plane of observation and calculation of the width of the central peak of the autocorrelation of the speckle pattern according to the method described above. Each process was carried out using 6000 pixels and took approximately one minute using a two-core computer running at 1.8 GHz each. As indicated above, we used $A = 200$ μm, $\lambda = 0.6328$ μm and $z = 1$ m. In the following

Metrol. Meas. Syst., Vol. 27 (2020), No. 1, pp. 103–117
DOI: 10.24425/amms.2020.131715

Table 1. Data corresponding to the generating function I.

Generating function I: $f(x) = \exp\left[-\left(\frac{\sqrt{x^2}}{L}\right)^{2\alpha}\right]$; $\alpha = 1.2$					
	$L = 3.0\ 10^{-6}$ (m)	$L = 3.2\ 10^{-6}$ (m)	$L = 3.4\ 10^{-6}$ (m)	$L = 3.6\ 10^{-6}$ (m)	$L = 3.8\ 10^{-6}$ (m)
Roughness 1×10^{-7} (m)	Speckle width. 1×10^{-3} (m)				
1.0	6.000	6.619	6.526	5.753	5.926
1.2	6.206	5.906	6.126	5.959	6.419
1.4	6.473	5.540	6.133	6.266	6.033
1.6	6.066	6.286	5.986	6.433	5.880
1.8	6.160	6.013	5.860	5.573	6.226

Table 2. Data corresponding to the generating function II.

Generating function II: $f(x) = \exp\left[-\left(\frac{\sqrt{x^2}}{L}\right)^{2\alpha}\right]$; $\alpha = 0.8$					
	$L = 3.0\ 10^{-6}$ (m)	$L = 3.2\ 10^{-6}$ (m)	$L = 3.4\ 10^{-6}$ (m)	$L = 3.6\ 10^{-6}$ (m)	$L = 3.8\ 10^{-6}$ (m)
Roughness 1×10^{-7} (m)	Speckle width. 1×10^{-3} (m)				
1.0	6.130	5.945	6.075	6.053	6.052
1.2	5.980	5.972	6.188	6.085	6.022
1.4	6.052	5.990	6.067	6.157	5.990
1.6	6.022	5.970	6.108	6.100	6.005
1.8	6.063	6.147	6.007	6.032	5.990

Table 3. Data corresponding to the generating function III.

Generating function III: $f(x) = \left[1 + \frac{1}{N}\left(\frac{x}{L}\right)^2\right]^{-N}$; $N = 6000$					
	$L = 3.0\ 10^{-6}$ (m)	$L = 3.2\ 10^{-6}$ (m)	$L = 3.4\ 10^{-6}$ (m)	$L = 3.6\ 10^{-6}$ (m)	$L = 3.8\ 10^{-6}$ (m)
Roughness 1×10^{-7} (m)	Speckle width. 1×10^{-3} (m)				
1.0	6.032	6.192	6.043	6.072	5.988
1.2	6.020	6.042	5.970	6.073	6.010
1.4	6.027	6.107	6.012	6.078	5.957
1.6	6.025	6.178	6.000	5.958	6.042
1.8	6.107	6.053	6.097	6.063	6.100

Tables 1–4, the averages of the autocorrelation widths corresponding to each generating function are presented.

In each of Tables 1–4 a generating function has $K = 5$ columns. Each column corresponds to a different L value. There are $M = 5$ rows for each generating function; each row corresponding

Table 4. Data corresponding to the generating function IV.

Generating function IV: $f(x) = J_0\left(\frac{x}{L}\right)$					
	$L = 3.0\ 10^{-6}$ (m)	$L = 3.2\ 10^{-6}$ (m)	$L = 3.4\ 10^{-6}$ (m)	$L = 3.6\ 10^{-6}$ (m)	$L = 3.8\ 10^{-6}$ (m)
Roughness 1×10^{-7} (m)	Speckle width. 1×10^{-3} (m)				
1.0	6.003	6.278	5.903	6.007	6.290
1.2	6.147	5.857	6.143	6.000	6.193
1.4	6.025	6.090	6.292	5.902	6.138
1.6	5.987	6.287	6.273	6.108	5.930
1.8	6.152	6.125	6.183	6.122	6.105

to a different vertical RMS height. As there are four different generating functions, we introduce the variable $NN = 4$ to represent the number of generating functions or, equivalently, the number of tables.

For the calculations, it is necessary to construct an overall single table, formed by concatenating each one of the above tables at the right of the other. This general table has a total of $N = NN \times K = 20$ columns. Under this assumption we can refer to each entry in this general table as $x_{p,s}$, where $p = 1, 2, ..M$ and $s = 1, 2, ..N$. An entry $x_{p,s}$ in the general table can be related to an entry in a table that corresponds to a specific generating function by the parameter denoted as $x_{p,q,k} = x_{p,(q-1)K+k}$, where $q = 1, 2, ..NN$ and $k = 1, 2, ..K$. Equivalently, in the parameter $x_{p,q,k}$ the sub-indexes (p, q, k) represent an entry corresponding to an RMS value, a generating function and an L value respectively and enables to describe the corresponding ANOVA and R&R calculations.

We will follow the well-established ANOVA model known as "two-factor factorial with random factors". This is a two-way model with interactions where the parameters are chosen randomly. This model, as indicated in [18] is stricter and more exhaustive for examining main effects even in the presence of interactions as compared with models with fixed effects. To attain the described two-way ANOVA, following [19], we propose:

$$x_{p,q,k} = \mu + \alpha_p + \beta_q + \gamma_{p,q} + \varepsilon_{p,q,k}\ . \tag{8}$$

In (8), α_p, β_q, $\gamma_{p,q}$, and $\varepsilon_{p,q,k}$ are random variables with zero mean and variances σ_α^2, σ_β^2, σ_γ^2, and σ^2, respectively. Additionally, $E\{\mu\} = \mu$, where the symbol $E\{\ .\ \}$ represents an expected value.

In the following Table 5, there are presented the required ANOVA mean value parameters.

Table 5. Mean value parameters for ANOVA.

Mean value for each generating function at row *p*	**Mean column value for each generating function**	**Mean row value of the four generating functions at row *p***	**Mean total value of all the entries**
$y_{p,q} = \frac{1}{K}\sum_{k=1}^{K} x_{p,q,k}$	$XCMM_q = \frac{1}{M}\sum_{p=1}^{M} y_{p,q}$	$XRM_p = \frac{1}{NN}\sum_{q=1}^{NN} y_{p,q}$	$XMT = \frac{1}{NN}\sum_{q=1}^{NN} XCMM_q$

In Table 6, using the data from Tables 1–4, the following required mean parameters are obtained.

Metrol. Meas. Syst., Vol. 27 (2020), No. 1, pp. 103–117
DOI: 10.24425/mms.2020.131715

Table 6. Required measured mean values as defined in Table 5.

1×10^{-3} m					
$XCMM_q$	6.094	6.048	6.050	6.102	
XRM_p	6.094	6.065	6.066	6.082	6.058
XMT	6.073				

The data of Table 6 can now be used in the ANOVA sum of squares of parameters and their corresponding mean squares given in the following Table 7.

Table 7. Definition of sum and mean of squares of parameters.

Sum of squares	**Mean of squares**
$SSA = KNN \sum_{p=1}^{M} \left(XRM_p - XMT\right)^2$	$MSA = \dfrac{SSA}{M-1}$
$SSB = KM \sum_{q=1}^{NN} \left(XCMM_q - XMT\right)^2$	$MSB = \dfrac{SSB}{NN-1}$
$SSAB = K \sum_{p=1}^{M} \sum_{q=1}^{NN} \left(y_{p,q} - XCMM_q - XRM_p + XMT\right)^2$	$MSAB = \dfrac{SSAB}{(NN-1)(M-1)}$
$SSE = \sum_{k=1}^{K} \sum_{p=1}^{M} \sum_{q=1}^{NN} \left(x_{p,(q-1)K+k} - y_{p,q}\right)^2$	$MSE = \dfrac{SSE}{NN(K-1)M}$

It is straightforward but lengthy to demonstrate the following relations given in Table 8 [17].

Table 8. Expected square values.

$E\{MSA\} = \sigma^2 + KNN\sigma_\alpha^2 + K\sigma_\gamma^2$
$E\{MSB\} = \sigma^2 + KM\sigma_\beta^2 + K\sigma_\gamma^2$
$E\{MSAB\} = \sigma^2 + K\sigma_\gamma^2$
$E\{MSE\} = \sigma^2$

Using Table 7 and the data from Tables 1–4 the results of the following Table 9 are obtained.

Table 9. Measured mean and sum of squares.

(m^2)	
$SSA = 1.662 \times 10^{-8}$	$MSA = 4.155 \times 10^{-9}$
$SSB = 6.114 \times 10^{-8}$	$MSB = 2.038 \times 10^{-8}$
$SSAB = 1.273 \times 10^{-7}$	$MSAB = 1.060 \times 10^{-8}$
$SSE = 2.286 \times 10^{-6}$	$MSE = 2.857 \times 10^{-8}$

The mean values given in Table 9 will be used in the following equations for calculating repeatability r, reproducibility R and gage repeatability-and-reproducibility $R\&R$:

$$r = \sigma = \sqrt{MSE}, \tag{9}$$

$$R = \sqrt{\sigma_\beta^2 + \sigma_\gamma^2} = \sqrt{\frac{MSB}{kM} + \frac{(M-1)}{KM}MSAB - \frac{MSE}{K}}, \tag{10}$$

$$R\&R = \sqrt{\sigma^2 + \sigma_\beta^2 + \sigma_\gamma^2} = \sqrt{\frac{MSB}{kM} + \frac{(M-1)}{KM}MSAB + \frac{(K-1)}{K}MSE}. \tag{11}$$

In a special case of (10), when the data are highly concentrated around the mean, the radicand approaches to zero or it may even be negative. In this particular case, the value assigned to R is zero, see for example [20].

Using (9)–(11) and the data from Table 9 the following results are obtained:

Table 10. Repeatability, reproducibility and gage $R\&R$.

$r = 1.69 \times 10^{-4}$ m	$R = 0$ (Negative radicand)	$R\&R = 1.59 \times 10^{-4}$ m

The results given in Table 10 are complemented with corresponding ANOVA F-tests. The F-distribution is given as:

$$F(N_1, N_2, x_0) = \frac{\Gamma\left(\frac{N_1+N_2}{2}\right)}{\Gamma\left(\frac{N_1}{2}\right)\Gamma\left(\frac{N_2}{2}\right)}\left(\frac{N_1}{N_2}\right)^{\frac{N_1}{2}}\int_0^{x_0}\frac{x^{\frac{N_1}{2}-1}}{\left(\frac{N_1}{N_2}x+1\right)^{\frac{N_1+N_2}{2}}}\mathrm{dx}. \tag{12}$$

Table 11 enables to compare the measured F values with their corresponding x_0 values obtained by means of (12), setting a confidence interval of 95%, equivalently, $F(N_1, N_2, x_0) = 0.95$.

Table 11. Measured F values and their corresponding x_0 values.

Measured F values	**Degrees of freedom**	$F(N_1, N_2, x_0) = 0.95$
$FA = MSA/MSAB = 0.3918$	$N_1 = 4$, $N_2 = 12$	$x_0 = 3.260$
$FB = MSB/MSE = 0.7133$	$N_1 = 3$, $N_2 = 80$	$x_0 = 2.719$
$FAB = MSAB/MSE = 0.3712$	$N_1 = 12$, $N_2 = 80$	$x_0 = 1.875$

Table 11 contains relevant information. The three measured F quantities are smaller than their corresponding x_0 values. As a consequence, it is not possible to reject the null-hypothesis. Thus, we conclude that the ample differences on the characteristics of the random rough surfaces considered do not affect the average speckle width of the propagated intensity speckle patterns calculated by means of the Fresnel diffraction integral. Neither the autocorrelation surface length of the rough surfaces nor their different vertical RMS heights affected the average speckle width. This result may be attributed to the quadratic phase in the Fresnel diffraction integral as it averages, upon propagation, the phase of the reflected beam modulated by the main structural characteristics of the rough surfaces such as asperity, roughness and waviness spacing.

The above one-dimensional study can, in principle, be extended to two dimensions. To carry out this task it is necessary to generate two-dimensional surfaces with random vertical heights on the initial plane and then calculate the propagation of the reflected beam up to a plane of observation by means of the two-dimensional discrete Fresnel diffraction integral. However, the processing time at these conditions would dramatically increase, making it necessary to devise

Metrol. Meas. Syst., Vol. 27 (2020), No. 1, pp. 103–117
DOI: 10.24425/amms.2020.131715

an alternative approach to obtain some insight into whether the above results are valid in two dimensions; therefore, we made use of the following approach. We generated one-dimensional distributions exhibiting random vertical heights arranged on the initial plane in four different directions: 0, 45, 90 and 135 degrees as the one shown in Fig. 6. For our purposes, these distributions may be visualized as linear slices or sub-samples of random surfaces spatially limited on the initial plane by a circular aperture.

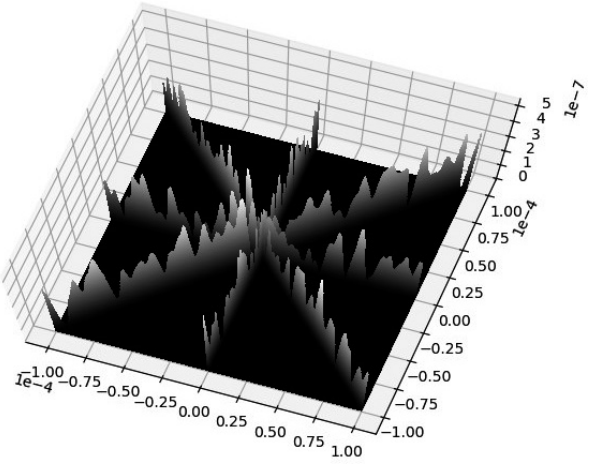

Fig. 6. One of the randomly generated sliced surfaces as described in the text (units in m).

We now use the two-dimensional discrete Fresnel diffraction integral to calculate the propagation of the reflected beam on the sliced surfaces along one axis on the plane of observation. For brevity, we will refer to this method as a 2D-sliced approach. Fig. 7 shows one of the obtained intensity profiles.

In Fig. 8 there is shown a normalized autocorrelation corresponding to the profile plotted in Fig. 7.

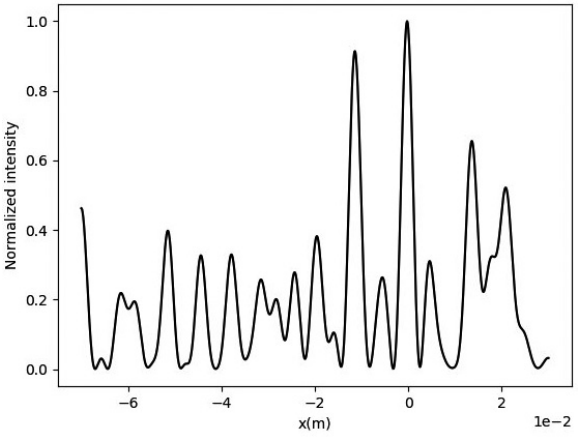

Fig. 7. A normalized intensity profile along one axis on the plane of observation of an illuminating beam reflected from one of the generated surfaces obtained with the 2D-sliced approach.

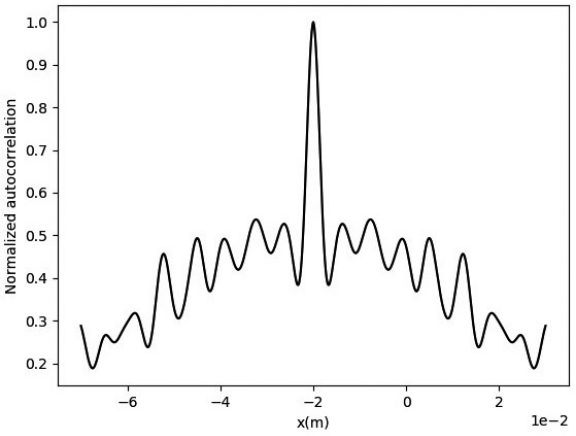

Fig. 8. A normalized autocorrelation for the speckle pattern plotted in Fig. 7.

In Tables 12–15, there are shown the speckle widths obtained using the 2D-sliced approach.

Table 12. Data corresponding to the generating function I using the 2D-sliced approach.

Generating function I: $f(x) = \exp\left[-\left(\frac{\sqrt{x^2}}{L}\right)^{2\alpha}\right]$; $\alpha = 1.2$					
	$L = 3.0\ 10^{-6}$ (m)	$L = 3.2\ 10^{-6}$ (m)	$L = 3.4\ 10^{-6}$ (m)	$L = 3.6\ 10^{-6}$ (m)	$L = 3.8\ 10^{-6}$ (m)
Roughness 1×10^{-7} (m)	Speckle width. 1×10^{-3} (m)				
1.0	8.817	10.022	10.017	8.767	8.800
1.2	7.467	8.600	8.355	7.633	7.783
1.4	8.967	9.900	7.850	8.516	8.016
1.6	9.000	9.417	8.533	9.783	9.933
1.8	9.517	9.983	8.400	7.516	8.050

Table 13. Data corresponding to the generating function II using the 2D-sliced approach.

Generating function II: $f(x) = \exp\left[-\left(\frac{\sqrt{x^2}}{L}\right)^{2\alpha}\right]$; $\alpha = 0.8$					
	$L = 3.0\ 10^{-6}$ (m)	$L = 3.2\ 10^{-6}$ (m)	$L = 3.4\ 10^{-6}$ (m)	$L = 3.6\ 10^{-6}$ (m)	$L = 3.8\ 10^{-6}$ (m)
Roughness 1×10^{-7} (m)	Speckle width. 1×10^{-3} (m)				
1.0	9.511	9.777	8.911	9.844	7.511
1.2	9.177	9.733	8.311	7.022	7.688
1.4	7.911	8.067	6.711	7.622	7.577
1.6	8.755	8.555	9.555	7.022	8.577
1.8	9.155	9.533	7.377	9.200	9.311

Metrol. Meas. Syst., Vol. 27 (2020), No. 1, pp. 103–117
DOI: 10.24425/mms.2020.131715

Table 14. Data corresponding to the generating function III using the 2D-sliced approach.

Generating function III: $f(x) = \left[1 + \frac{1}{N}\left(\frac{x}{L}\right)^2\right]^{-N}$; $N = 6000$					
	$L = 3.0\ 10^{-6}$ (m)	$L = 3.2\ 10^{-6}$ (m)	$L = 3.4\ 10^{-6}$ (m)	$L = 3.6\ 10^{-6}$ (m)	$L = 3.8\ 10^{-6}$ (m)
Roughness 1×10^{-7} (m)	Speckle width. 1×10^{-3} (m)				
1.0	8.528	8.444	9.244	8.422	8.111
1.2	9.999	8.999	8.622	7.555	9.333
1.4	8.733	9.178	8.200	7.244	9.755
1.6	8.578	7.955	9.489	10.155	7.577
1.8	8.111	10.012	9.799	8.577	8.977

Table 15. Data corresponding to the generating function IV using the 2D-sliced approach.

Generating function IV: $f(x) = J_0\left(\frac{x}{L}\right)$					
	$L = 3.0\ 10^{-6}$ (m)	$L = 3.2\ 10^{-6}$ (m)	$L = 3.4\ 10^{-6}$ (m)	$L = 3.6\ 10^{-6}$ (m)	$L = 3.8\ 10^{-6}$ (m)
Roughness 1×10^{-7} (m)	Speckle width. 1×10^{-3} (m)				
1.0	9.867	8.422	8.533	7.133	10.000
1.2	9.222	9.177	9.133	8.022	8.577
1.4	9.044	8.000	9.200	8.889	8.777
1.6	7.599	7.911	8.822	7.622	8.755
1.8	7.600	8.999	8.555	7.600	9.933

It should be noticed that the speckle widths in Tables 12–15 are greater than those obtained in Tables 1–4. This result is in accordance with [15], where it is analytically demonstrated that for the case of surfaces with random Gaussian distributions, spatially limited by a circular aperture, the average speckle widths are approximately 1.2 times greater than the widths of the one-dimensional case.

The processing time for each two-dimensional calculation took approximately 4 minutes and each entry in a table was obtained by averaging three of these calculations. Tables 16–19 show the obtained ANOVA and *R&R* results.

Table 16. Mean values obtained as defined in Table 5 using the 2D-sliced approach.

1×10^{-3} m					
$XCMM_q$	8.785	8.496	8.784	8.616	
XRM_p	8.934	8.520	8.408	8.679	8.810
XMT	8.6704				

Table 19 reveals that the three measured F values are smaller than their corresponding x_0 values. Thus, similarly to the one-dimensional case, it is not possible to reject the null-hypothesis. As a consequence, it appears that the aforementioned one-dimensional results can be extended to two dimensions.

Table 17. Measured mean and sum of squares obtained with the 2D-sliced approach.

(m^2)	
$SSA = 3.612 \times 10^{-6}$	$MSA = 9.029 \times 10^{-7}$
$SSB = 1.485 \times 10^{-6}$	$MSB = 4.949 \times 10^{-7}$
$SSAB = 1.229 \times 10^{-5}$	$MSAB = 1.024 \times 10^{-6}$
$SSE = 5.479 \times 10^{-5}$	$MSE = 6.848 \times 10^{-7}$

Table 18. Repeatability, reproducibility and gage $R\&R$ obtained with the 2D-sliced approach.

$r = 8.28 \times 10^{-4}$ m	$R = 2.16 \times 10^{-4}$ m	$R\&R = 8.55 \times 10^{-4}$ m

Table 19. Measured F values and their corresponding x_0 values obtained with the 2D-sliced approach.

Measured F values	**Degrees of freedom**	$F(N_1, N_2, x_0) = 0.95$
$FA = MSA/MSAB = 0.8816$	$N_1 = 4$, $N_2 = 12$	$x_0 = 3.260$
$FB = MSB/MSE = 0.7227$	$N_1 = 3$, $N_2 = 80$	$x_0 = 2.719$
$FAB = MSAB/MSE = 1.4956$	$N_1 = 12$, $N_2 = 80$	$x_0 = 1.875$

4. Conclusions

We have presented an illustrative working example of an ANOVA gage R&R study for speckle statistics. Four types of random rough surfaces were generated with different statistical characteristics. The intensity speckle patterns produced by the reflection of a spatially-limited coherence illuminating beam on the generated surfaces were calculated on a plane of observation by means of the discrete Fresnel diffraction integral. We verified that, on the plane of observation, all the accomplished intensity histograms exhibited the well-known exponentially decreasing behavior. To assure that all the measurements were performed in strictly identical conditions an automated method was implemented. The ANOVA and R&R results showed satisfactory values of repeatability and gage-reproducibility. The corresponding F factors were adequate within a confidence interval of 95%. Thus, the ANOVA and R&R results did not give any evidence for rejecting the null hypothesis. In consequence, random rough surfaces exhibiting different random characteristics do not appear to affect the average speckle width or the exponential decreasing behavior.

Acknowledgements

We are grateful to two reviewers that anonymously revised our manuscript providing us with valuable suggestions.

The authors thank CONACYT for their partial support.

Metrol. Meas. Syst., Vol. 27 (2020), No. 1, pp. 103–117
DOI: 10.24425/mms.2020.131715

References

[1] *https://www.iso.org/obp/ui/#iso:std:iso:5725:-1:ed-1:v1:en:sec:B* (1994).

[2] Joenathan, C., Franze, B., Haible, P., Tiziani, H. J. (1998). Speckle interferometry with temporal phase evaluation for measuring large-object deformation. *Appl. Opt.*, 37(13), 2608–2614.

[3] Léger, D., Mathieu, E., Perrin, J.C. (1975). Optical surface roughness determination using speckle correlation technique. *Appl. Opt.*, 14(4), 872–877.

[4] Tango, W.J., Davis, J., Thompson, R.J., Brown, R.H. (1979). A 'Narrabri'Binary Star Resolved by Speckle Interferometry. *Publ. Astron. Soc. Aust.*, 3(5), 323–324.

[5] Junior, R.A.B., Silva, B.O., Rabelo, G., Costa, R.M., Enes, A.M., Cap, N., Horgan, G. (2007). Reliability of biospeckle image analysis. *Opt. Lasers Eng.*, 45(3), 390–395.

[6] Yokoi, N., Aizu, Y., Uozumi, J. (2018). Fractality of biospeckle pattern observed in blood coagulation process. In Biomedical Imaging and Sensing Conference, *SPIE.*, 10711, 107111V.

[7] Summers, J.E., Soukup, R.J., Gragg, R.F. (2005). Characterization and fabrication of synthetic rough surfaces for acoustical scale-model experiments. *Naval Research Lab Washington Dc Acoustics Div*, NRL/MR-MM/7140-05-8871.

[8] Equis, S., Jacquot, P. (2006). Simulation of speckle complex amplitude: advocating the linear model. Speckle06: Speckles, From Grains to Flowers, *SPIE.*, 6341, 634138.

[9] Guérin, C.A. (2002). Scattering on rough surfaces with alpha-stable non-Gaussian height distributions. *Wave Random Media*, 12(3), 293–306.

[10] Wu, S.C., Chen, M.F., Fung, A.K. (1988). Non-Gaussian surface generation. *IEEE Trans. Geosci. Remote Sens.*, 26(6), 885–888.

[11] Wu, S.C., Chen, M.F., Fung, A.K. (1988). Scattering from non-Gaussian randomly rough surfaces-cylindrical case. *IEEE Trans. Geosci. Remote Sens.*, 26(6), 790–798.

[12] Patir, N. (1978). A numerical procedure for random generation of rough surfaces. *Wear*, 47(2), 263–277.

[13] Cheng, C., Liu, C., Teng, S., Zhang, N., Liu, M. (2002). Half-width of intensity profiles of light scattered from self-affine fractal random surfaces and simulational verifications. *Phys. Rev. E.*, 65(6), 061104.

[14] Uchida, K., Honda, J., Yoon, K.Y. (2011). An algorithm for rough surface generation with inhomogeneous parameters. *JACT*, 5(2), 259–271.

[15] Goodman, J.W. (2008). *Introduction to Fourier optics*. Roberts and Company publishers, 63–88.

[16] Dainty, J.C. (1975). *Laser speckle and related phenomena*. Springer-Verlag Berlin Heidelberg New York, 9–74.

[17] Brown, J.C., Puckette, M.S. (1989). Calculation of a "narrowed" autocorrelation function. *J. Acoust. Soc. Am.*, 85(4), 1595–1601.

[18] Stryhn, H. (2006). Notes on Linear Mixed Models. *Atlantic Veterinary College*, *PEI*, 1–15.

[19] Montgomery, D.C. (2013). *Design and analysis of experiments*. John Wiley & Sons, Inc., 573–601.

[20] Vardeman, S.B., Jobe, J.M. (2016). *Statistical Methods for Quality Assurance*. Springer-Verlag New York, 62–75.